Proceedings of ASME Turbo Expo 2008: Power for Land, Sea and Air
GT2008
June 9-13, 2008, Berlin, Germany

GT2008 - 50295

EFFECT OF RADIAL LOCATION OF NOZZLES ON PERFORMANCE OF PRE-SWIRL SYSTEMS

Paul Lewis p.r.lewis@bath.ac.uk
Mike Wilson m.wilson@bath.ac.uk
Gary Lock g.d.lock@bath.ac.uk
J. Michael Owen j.m.owen@bath.ac.uk

Dept of Mechanical Engineering
University of Bath
Bath BA2 7AY
United Kingdom

ABSTRACT

This paper investigates the effect of the radial location of the inlet nozzles on the performance of a direct-transfer pre-swirl system in a rotor-stator wheel-space. A commercial code is used to solve the Reynolds Averaged Navier Stokes (RANS) equations using a high-Reynolds-number k-ε / k-ω turbulence model with wall functions near the boundary. The 3D steady state model has previously been validated against experimental results from a scale model of a gas turbine rotor-stator system. Computations are performed for three inlet-to-outlet radius ratios, r_p/r_b = 0.8, 0.9 and 1.0, a range of pre-swirl ratios, $0.5 < \beta_b < 2.0$, and varying flow parameter, $0.12 < \lambda_T < 0.36$. The rotational Reynolds number for each case is 10^6.

The flow structure in the wheel-space and in the region around the receiver holes for each inlet radius is related to the swirl ratio. The performance of the system is quantified by two parameters: the discharge coefficient for the receiver holes ($C_{d,b}$) and the adiabatic effectiveness for the system ($\Theta_{b,ad}$).

As in previous work, the discharge coefficient is found to reach a maximum when the rotating core of fluid is in synchronous rotation with the receiver holes. As the radius ratio is increased this condition can be achieved with a smaller value for pre-swirl ratio β_b. A simple model is presented to estimate the discharge coefficient based on the flow rate and swirl ratio in the system.

The adiabatic effectiveness of the system increases linearly with pre-swirl ratio but is independent of flow rate. For a given pre-swirl ratio, the effectiveness increases as the radius ratio increases. Computed values show good agreement with analytical results. Both performance parameters show improvement with increasing inlet radius ratio, suggesting that for an optimum pre-swirl configuration an engine designer would place the pre-swirl nozzles at a high radius.

NOMENCLATURE

a , b	rotor inner radius, rotor outer radius
A ,B	combined free and forced vortex coefficients
A_b	receiver hole area
c_w	non-dimensional mass flow rate ($= \dot{m} / \mu b$)
c_p	specific heat capacity at constant pressure
C_d	discharge coefficient
C_M	disc moment coefficient ($= M / \frac{1}{2}\rho\Omega^2 b^5$)
G	gap ratio (= s / b)
$\dot{m}$	mass flow rate
M	moment on one side of the disc
Re_ϕ	rotational Reynolds number ($= \rho\Omega b^2/\mu$)
r	radius
r_p, r_b	radii of pre-swirl nozzles and receiver holes
s	rotor-stator separation distance
T	temperature
V	velocity
x	non-dimensional radius ($= r / b$)
α	flow angle relative to axial direction
β	swirl ratio ($= V_\phi / \Omega r$)
β_b	pre-swirl ratio based on r_b ($= V_{\phi,p} / \Omega r_b$)
β_p	pre-swirl ratio based on r_p ($= V_{\phi,p} / \Omega r_p$)
γ	ratio of specific heats
θ	inlet nozzle angle to the tangential direction
$\Theta_{b,ad}$	adiabatic effectiveness ($c_p(T_{o,p}-T_{t,b})/\frac{1}{2}\Omega^2 r_b^2$)

λ_T	turbulent flow parameter ($= c_w\, Re_\phi^{-0.8}$)
μ	dynamic viscosity
ρ	density
Ω	angular velocity of rotor

Subscripts

ad	adiabatic
b	blade-cooling
e	effective
i	isentropic value
max	maxium value
o	total value in stationary frame
out	at receiver hole outlet
p	pre-swirl
s	stator
t	total value in rotating frame
w	rotor
ϕ, r, z	circumferential, radial, axial direction
∞	value in core at z/s = 0.5, $r/r_b = 1$
1,2	upstream, downstream locations in streamtube

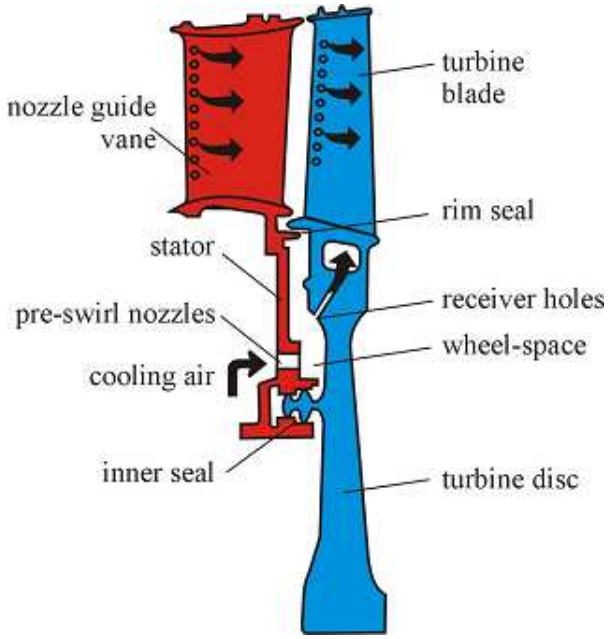

Fig 1 Simplified diagram of a direct-transfer pre-swirl system

INTRODUCTION

A simplified diagram of the so-called direct-transfer pre-swirl system, where the blade-cooling air is supplied to the rotating blades by stationary angled pre-swirl nozzles, is shown in Fig 1. The nozzles swirl the air, and this reduces the work done by the rotating turbine disc in accelerating the air to the disc speed. This consequently reduces the total temperature of the air entering the receiver holes in the disc, Meierhofer and Franklin [1]. The designer is interested in calculating the pressure drop and cooling effectiveness of the pre-swirl system, and there is also a need to understand the heat transfer between the cooling air and the turbine disc.

Heat transfer in a direct transfer rig was studied experimentally and computationally by Wilson et al. [2]. Total temperature probes were used to measure the temperature of the air entering the receiver holes, which was consistently under-predicted by axisymmetric CFD computations.

Geis et al. [3] made measurements of adiabatic effectiveness which showed that the measured values of $T_{t,b}$, the total temperature of the air in the rotating frame of reference entering the receiver holes, were significantly higher than the values predicted from their ideal model. Chew et al. [4] made numerical simulations that were in good agreement with results from both the 'Karlsruhe' pre-swirl rig used by Geis et al. and a pre-swirl rig at Sussex University. Chew et al. and Farzaneh-Gord et al. [5] derived independently theoretical models for the adiabatic effectiveness.

Dittmann et al. [6] measured the discharge coefficients for the pre-swirl nozzles and receiver holes in a direct-transfer system, and Yan et al. [7] measured the discharge coefficients for receiver holes.

Lewis et al. [8] carried out a combined computational and experimental study of a direct-transfer system. The computed adiabatic effectiveness was in good agreement with the theoretical expression derived by Farzaneh-Gord et al., and the computed values of $C_{d,b}$, the discharge coefficient for the receiver holes, reached a maximum value at a critical value of β_p, the pre-swirl ratio of the cooling air.

Lewis et al studied a system having the pre-swirl inlet at a lower radius than that of the receiver holes (as illustrated in Fig. 1), while the 'Karlsruhe' rig used by Dittman et al involved pre-swirl nozzles and receiver holes at the same high radius. Jarzombek et al [9] studied computationally a configuration with the pre-swirl nozzles located radially outward of the receiver holes, finding the flow to conform to free vortex behaviour. It is the object of the present paper to determine the effect of the radial location of the pre-swirl nozzles on system performance.

In previous papers by the authors, in which only one location for the pre-swirl nozzles was considered, the pre-swirl ratio β_p was defined as:

$$\beta_p = V_{\phi,p} / \Omega r_p \qquad (1)$$

In an engine, the total pressure upstream of the pre-swirl nozzles is fixed. If the static pressure in the core was also fixed then the pre-swirl velocity $V_{\phi,p}$ would be invariant with radius. Under these conditions, it is convenient to define a new pre-swirl ratio, β_b say, where:

$$\beta_b = V_{\phi,p} / \Omega r_b \qquad (2)$$

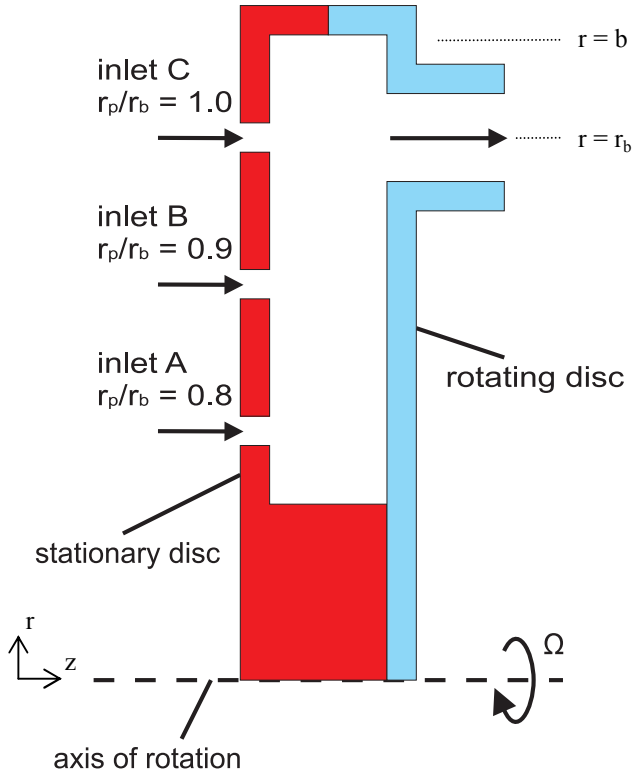

Fig. 2 Schematic diagram of the flow domain used for the computational study

such that β_b is invariant with r_p, which is the assumption made for the computations presented below. This will make it easier to identify the effect of nozzle location on pre-swirl performance. (As shown in the Appendix, the static pressure in the core does vary with radius, and this has an effect on β_b which reduces, but does not negate, the advantages of locating the pre-swirl nozzles at as high a radius as practicable.)

The computational method is described below, and subsequent sections consider the effect of nozzle location on the flow structure, the discharge coefficient for the receiver holes, the pressure drop in the system and the adiabatic effectiveness.

COMPUTATIONAL METHOD

The computational method and configuration is similar to that described in Lewis et al. [8], with adjustments made for multiple inlets; the salient details are included here for completeness. The computational domain, Fig. 2, is a 6^o section of a wheel-space bounded by a rotor and a stator disc with axial gap ratio G = 0.051. Cyclic symmetry is imposed at the circumferential boundaries. The system is sealed at its periphery (where b = 0.216 m) by a shroud attached to each disc, and the centre of the system is sealed by a stationary hub. Clearances between rotating and stationary surfaces are set to zero.

A cylinder, representing the blade cooling passage, of diameter 8 mm and length 10 mm is attached to the rotor at a radius r_b = 0.200 m and rotates with the disc. The pre-swirl nozzles are represented by an annular slot which can be placed at one of three radial locations such that r_p/r_b = 0.8, 0.9 or 1.0. The height of the annular slot is adjusted so that the pre-swirl inlet area remains the same at each of these three radial locations. The same set of values for inlet mass flow rate, in the range $0.12 < \lambda_T < 0.36$, is used for each configuration, and the pre-swirl ratio β_b is varied as a parameter. The rotational Reynolds number considered is $Re_\phi = 10^6$ (corresponding to a rotor disc speed of 3800 rpm).

The surface mesh for the geometry is created using a Delaunay triangulation with prismatic elements near the boundaries for better near wall resolution. An advancing front mesher is then used to resolve the volume.

CFX-10, a commercial 3D finite volume multi-grid computational fluid dynamics (CFD) package is used to solve the Reynolds Averaged Navier-Stokes (RANS) equations. The second order accurate advection scheme is based on the method of Barth and Jesperson [10]. The energy equation is solved including the viscous work term, and the effects of variable density are taken into account. Buoyancy effects within the wheel-space are ignored.

The turbulence model used is the high-Reynolds-number BSL model of Menter [11]. This is a blend of a k-ω formulation with wall functions in the near wall region, Wilcox [12], and a k-ε model away from the wall. This overcomes sensitivities to free stream turbulence levels experienced by k-ω models.

The equations were solved in the rotating frame such that a steady state analysis could be used. Axial and circumferential velocities were specified at the annular slot being used for the inlet. The two remaining slots in each analysis were treated as part of the solid stator. A static pressure boundary condition was used at the outlet.

FLOW STRUCTURE

The computed flow structure in the radial (r-z) plane for typical flow rates and pre-swirl ratios is shown in Fig. 3(a-c) for case where the inlet is located at r_p/r_b = 0.8, 0.9 and 1.0 respectively. The circumferential location ϕ of the plane shown coincides with the centre-line of the receiver hole. (There is little effect of circumferential location on the flow structure except in the immediate region of the receiver hole.) For r_p/r_b = 0.8 the inlet flow impinges upon the rotating disc and travels radially outwards, forming the rotor boundary layer. Radial inflow occurs on the stator and a pair of counter-rotating vortices can be observed inboard of the inlet.

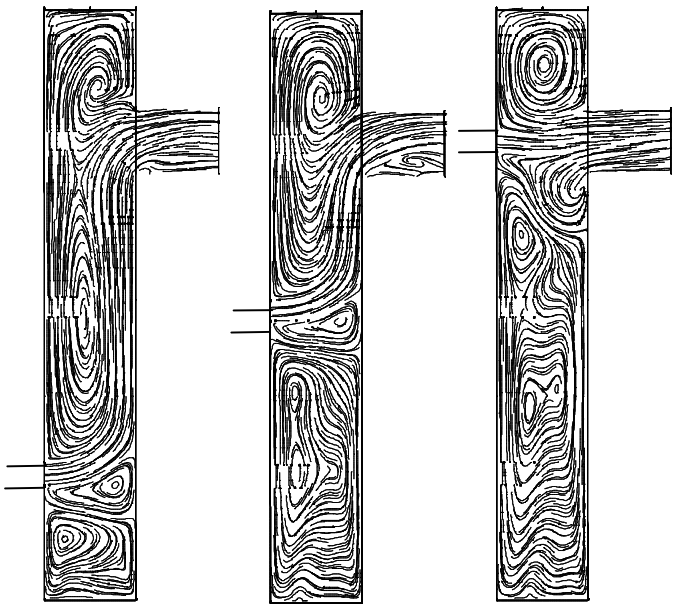

a) $r_p/r_b = 0.8$ b) $r_p/r_b = 0.9$ c) $r_p/r_b = 1.0$

Fig. 3 Computed flowfields in the axial-radial plane

As the inlet is moved radially outwards the circulation in the outer part of the system becomes more compressed. The pair of counter-rotating vortices inward of the inlet expands to fill the available space, the larger of the two vortices being that with outflow on the rotor.

The flow is most complex for the case when r_p/r_b is unity, Fig. 3(c). Some of the inlet flow enters the receiver holes directly, while the remaining flow impinges upon the region between the holes. The impinging flow spreads both radially inwards and radially outwards from the impingement region. The inward flow encounters the rotor boundary layer flow and separates from the disc, creating the small recirculation on the rotor side inward of the receiver hole.

Fig. 4 shows flow streamlines in the tangential (ϕ-z) plane at the receiver hole radius r_b in a frame of reference rotating at the speed of the rotor (in the left to right direction). In each image the stator is at the bottom and the receiver hole and outlet is at the top. The three columns represent the three inlet positions, r_p/r_b = 0.8, 0.9 and 1.0 respectively, and the rows represent increasing values of pre-swirl ratio.

For r_p/r_b = 0.8, Fig. 4(a) shows a case for which β_b = 0.40 and is therefore 'under-swirled'. The receiver hole rotates more quickly than the flow in the core, therefore the flow enters at an acute angle, separating at the leading edge of the hole and causing a recirculation inside the hole. As the pre-swirl ratio is increased the angle at which the flow enters the receiver hole tends towards the axial direction. At the point where synchronous rotation between the flow and the hole occurs the flow would be expected to flow axially into the receiver hole, as can be seen in Fig. 4(j), for which β_b = 1.6.

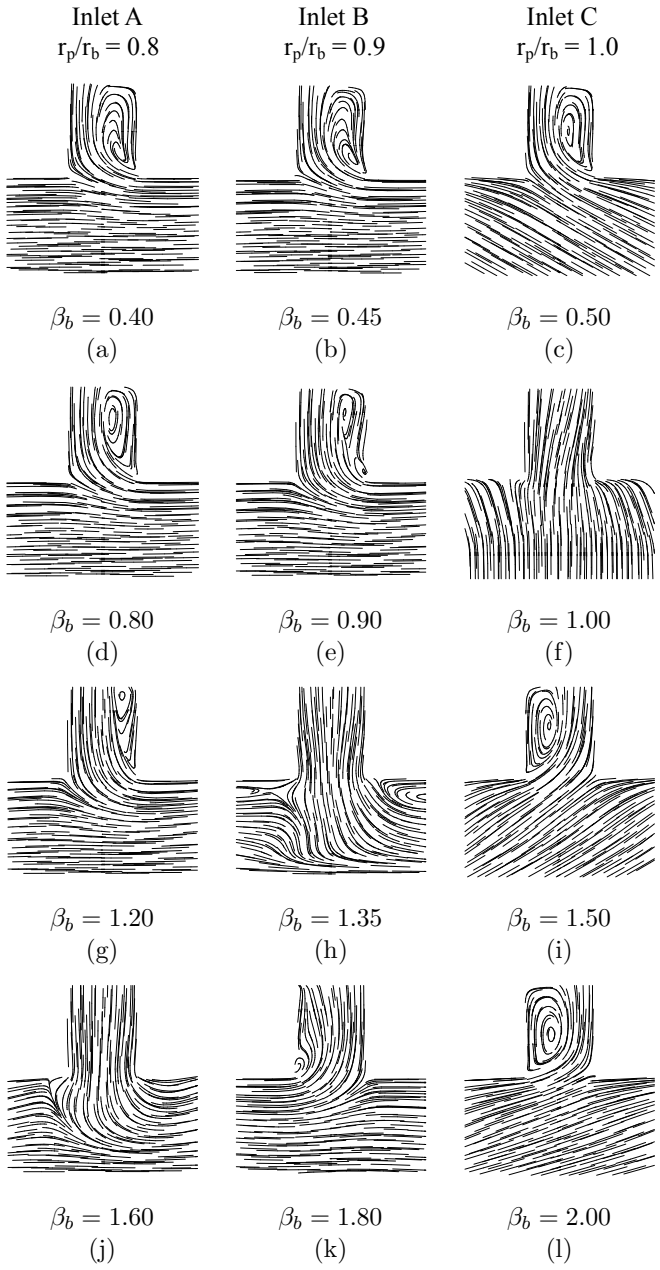

Fig. 4 Computed flow structure in the tangential plane at the receiver hole radius, in a frame of reference rotating with the rotor (direction of motion from left to right). $\lambda_T = 0.24$.

As the inlet radius is increased, the inlet pre-swirl ratio required to produce this synchronous rotation is reduced. For r_p/r_b = 0.9, synchronous rotation occurs when β_b = 1.35 as shown in Fig. 4(h) and for r_p/r_b = 1.0, when β_b = 1.0 as shown in Fig. 4(f). When the swirl ratio is increased further, or 'over-swirled', the flow rotates more quickly than the receiver hole, causing separation and a region of recirculation at the trailing edge of the hole.

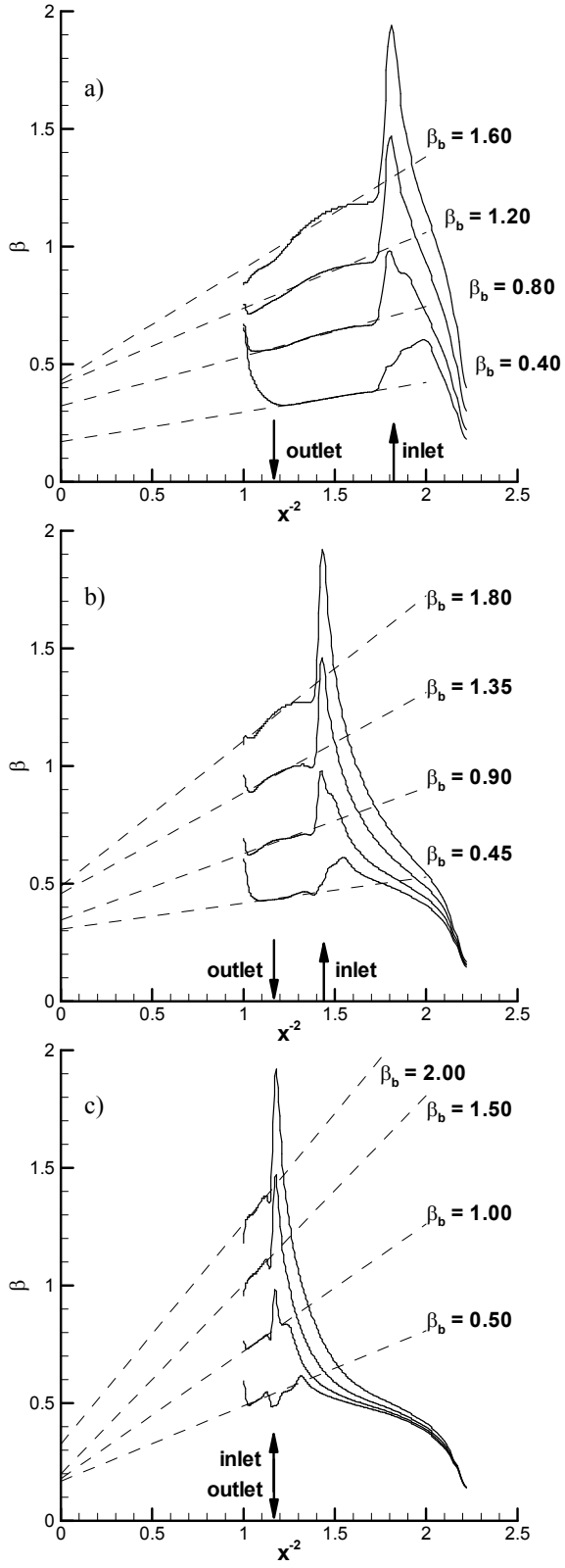

Fig. 5 Computed tangential velocity distributions on the axial mid-plane, a) $r_p/r_b = 0.8$, b) $r_p/r_b = 0.9$, c) $r_p/r_b = 1.0$

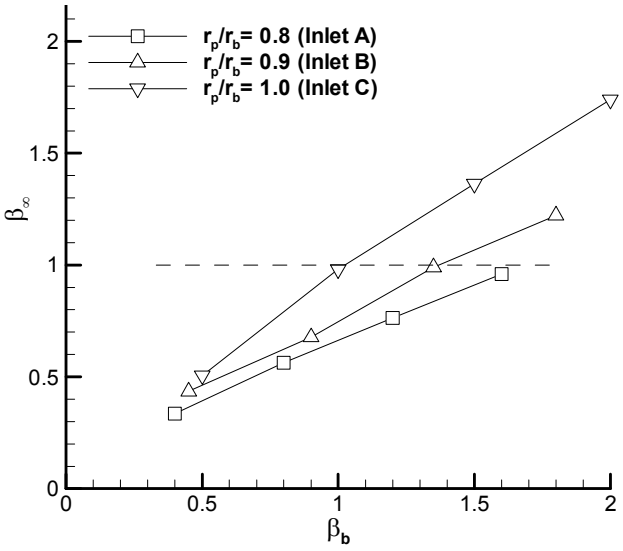

Fig. 6 Computed variation of β_∞ with β_b for the three inlet locations, $\lambda_T = 0.24$.

The variation of swirl ratio $\beta = V_\phi/\Omega r$ midway between the rotor and stator (z/s=0.5) and on a radial line midway between receiver holes is shown in Fig. 5. Fig. 5(a), (b) and (c) again correspond to the inlet at r_p/r_b = 0.8, 0.9 and 1.0 respectively. The horizontal axis is the non-dimensional radius x = r/b.

In each case a peak is seen in the swirl ratio at the inlet radius due to the high momentum inlet fluid. At higher radius (i.e. lower values of x^{-2}) there is a linear variation of β with x^{-2}, consistent with free vortex behaviour. The dashed line on each plot is a least squares best fit of the data in the linear region.

There is considerable uncertainty associated with the fit (especially as the region of linear behaviour becomes smaller), however these results suggest that the flow is related to a Rankine (combined free and forced) vortex, for which:

$$\beta = Ax^{-2} + B \qquad (3)$$

where A and B are constants. This behaviour was found by Mizaee et al [13] to occur in a rotating cavity with a stationary outer casing.

Fig. 6 shows the variation of swirl ratio in the core at the radius of the receiver hole, β_∞, with the pre-swirl ratio at inlet β_b. Each line represents a different inlet location and is approximately linear. Extrapolating back to the $\beta_b = 0$ condition, the value for β_∞ would be expected to lie between 0.43, the value for turbulent flow in a sealed rotor-stator system (see Owen and Rogers, [14]) and zero, due to the effect of a zero-swirl superposed flow on the swirl in the rotating core of fluid between the discs. It can be seen that a significant increase in inlet pre-swirl is required for the inlets at lower radii to achieve the synchronous rotation condition discussed above, and illustrated by the horizontal dashed line in Fig. 6.

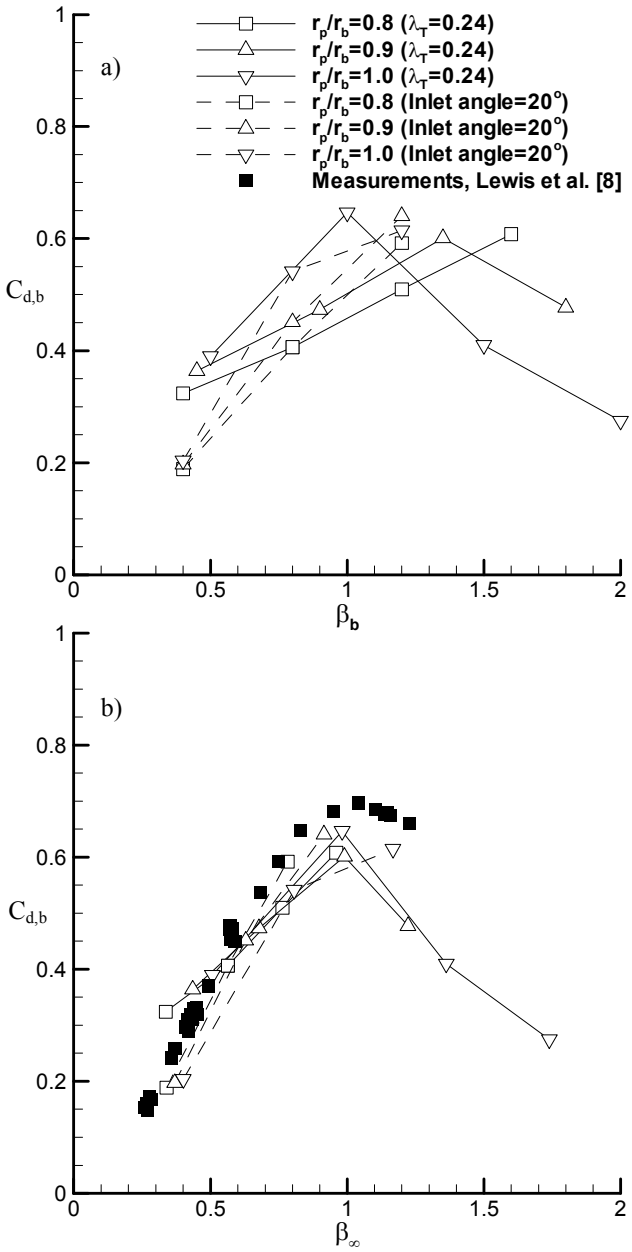

Fig. 7 Computed variation of discharge coefficient $C_{d,b}$ a) with β_b, b) with β_∞

DISCHARGE COEFFICIENT

The discharge coefficient $C_{d,b}$ is defined here as the ratio of the actual mass flow rate through the receiver holes $\dot{m}_b$ to the isentropic mass flow rate $\dot{m}_i$ such that:

$$C_{d,b} = \frac{\dot{m}_b}{\dot{m}_i} \tag{4}$$

The isentropic mass flow rate through the receiver holes was derived by Yan et al [7] using the First Law of Thermodynamics for an adiabatic system, taking into account the work done by or on the fluid as it passes from station 1 in the fluid core to station 2 in the receiver holes. It is given by:

$$\frac{\dot{m}_i}{A_b} = \rho_{0,1}\left(\frac{p_2}{p_{0,1}}\right)^{\frac{1}{\gamma}} \left\{ \begin{array}{l} \left(\frac{2\gamma}{\gamma-1}\right)\frac{p_{0,1}}{\rho_{0,1}}\left[1-\left(\frac{p_2}{p_{0,1}}\right)^{\frac{\gamma-1}{\gamma}}\right] \\ +\,2\Omega\left(r_2 V_{\phi,2} - r_1 V_{\phi,1}\right) - V_{\phi,2}^2 \end{array} \right\}^{1/2} \tag{5}$$

The first term inside the curly brackets is the standard result for compressible flow in a stationary nozzle; the second term is the work term resulting from the change of angular momentum of the air; the last term is due to the fact that the air in the receiver holes has an absolute tangential, as well as an axial, component of velocity. It should be noted that failure to use the correct equation for $\dot{m}_i$ can result in calculated values of $C_{d,b}$ exceeding unity, which is clearly nonsensical.

Fig. 7 shows this discharge coefficient calculated using locations 1 and 2 as a point in the core at the radius of the receiver holes and the outlet plane respectively. Fig 7a, where β_b is on the horizontal axis, clearly shows that to maximize the discharge coefficient for low radius inlets, the pre-swirl ratio must be greater than unity. The effect of varying pre-swirl ratio at a fixed non-dimensional flow rate λ_T (the equivalent of physically altering the inlet pre-swirl angle) is to produce a sharp change in the relationship between $C_{d,b}$ and β_b when the maximum value of $C_{d,b}$ is reached.

Lewis et al [8] presented computations and measurements, for the $r_p/r_b = 0.8$ configuration also considered here, for a fixed inlet flow angle of 20º to the tangential in the direction of rotation of the disc and variable flow rate. In this case, the inlet pre-swirl ratio is proportional to the non-dimensional flow rate λ_T used (at fixed Re_ϕ). Results for computations at this same fixed inlet flow angle (for $0.12 < \lambda_T < 0.36$) are also shown in Fig. 7a, and show a smaller effect of r_p/r_b on the variation of $C_{d,b}$ with β_b. Fig. 7b shows that, when the pre-swirl ratio is varied at a fixed value of λ_T, a nearly symmetric variation of $C_{d,b}$ around the point of synchronous rotation ($\beta_\infty = 1$) is obtained. (The values of inlet pre-swirl ratio β_b required to achieve synchronous rotation at the receiver hole radius are discussed above in connection with Fig. 4.) There is reasonably good agreement between the computations and the measurements made by Lewis et al for $r_p/r_b = 0.8$ and fixed inlet flow angle.

It was shown above that the effect of 'under-swirling ' or 'over-swirling' the core body of fluid caused the flow to enter the receiver hole at an angle to the axial direction. This means that the effective area of the receiver hole, as 'seen' by the flow, is reduced. It is logical that, since the flow rate is proportional to the orifice area, $C_{d,b}$ will reduce linearly as the effective area is reduced.

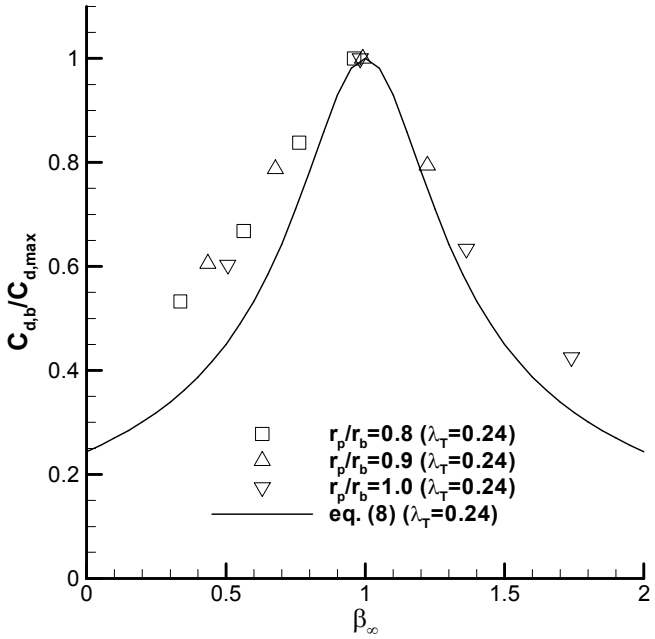

Fig. 8 Variation of $C_{d,b}/C_{d,max}$ with β_∞

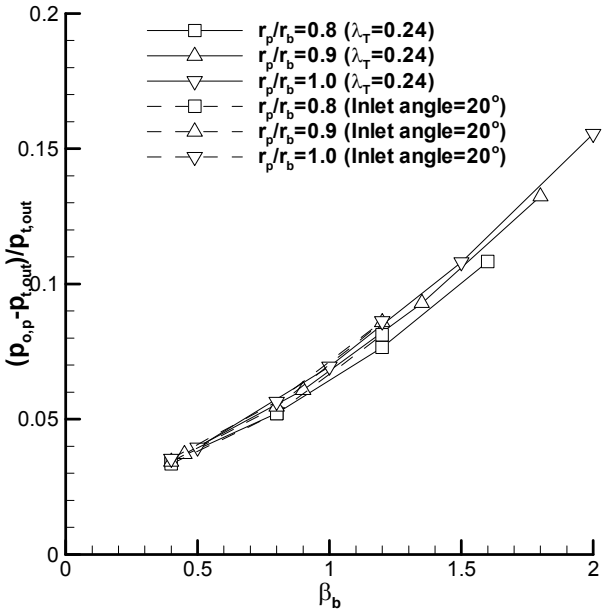

Fig. 9 Computed variation of pressure drop from pre-swirl inlet to receiver-hole outlet with β_b

The reduction in effective area A_e can be expressed as a function of the flow angle at the receiver hole, shown in eq. (6), where α is the flow angle measured from the axial direction.

$$\frac{A_e}{A_b} = \cos\alpha \tag{6}$$

An equation can be formed for α by considering the ratio of the tangential velocity in the rotating frame and the axial velocity. The radial component of velocity is ignored as a large volume of the flow enters the hole from the core rather than from the boundary layer and therefore has very low radial velocity (see Lewis et al discussion on 'direct' and 'indirect' routes). Hence:

$$\tan\alpha = \frac{\left|V_{\phi,\infty} - \Omega r_b\right|}{V_{z,b}} \tag{7a}$$

where:

$$V_{z,b} = \frac{\dot{m}_b}{\rho A_b} \tag{7b}$$

and

$$\left|V_{\phi,\infty} - \Omega r_b\right| = \left|\beta_\infty - 1\right| \Omega r_b \tag{7c}$$

Using the definition of λ_T given in the nomenclature it follows that

$$\frac{C_{d,b}}{C_{d,max}} = \frac{A_e}{A_b} = \frac{1}{\sqrt{1 + \left(\frac{A_b \rho \left|\beta_\infty - 1\right| \Omega r_b}{\mu b \lambda_T \, Re_\phi^{0.8}}\right)^2}} \tag{8}$$

where $C_{d,max}$ is the value of $C_{d,b}$ when $\beta_\infty = 1$.

Fig. 8 shows $C_{d,b}/C_{d,max}$ for a range of conditions and flow rates. The model underpredicts the computational data, which suggests that the predicted flow angle is too large, so that the predicted effective area is too small. At the entrance to the hole the circumferential velocity will be somewhere between that of the fluid in the core and that of the receiver hole.

Fig. 9 shows the total pressure loss through the system, using the total pressure in the stationary frame at inlet and in the rotating frame at outlet. This difference is largely independent of flow rate. There is a significant increase in pressure loss as the pre-swirl ratio is increased. Fig. 7a shows that the discharge coefficient for the receiver holes increases as the ratio r_p/r_b increases; Fig. 9 shows however that increasing r_p/r_b causes a slight increase in pressure drop.

ADIABATIC EFFECTIVENESS

The adiabatic effectiveness $\Theta_{b,ad}$ is defined as the non-dimensional change in total temperature between the nozzles in the stationary frame and the receiver holes in the rotating frame:

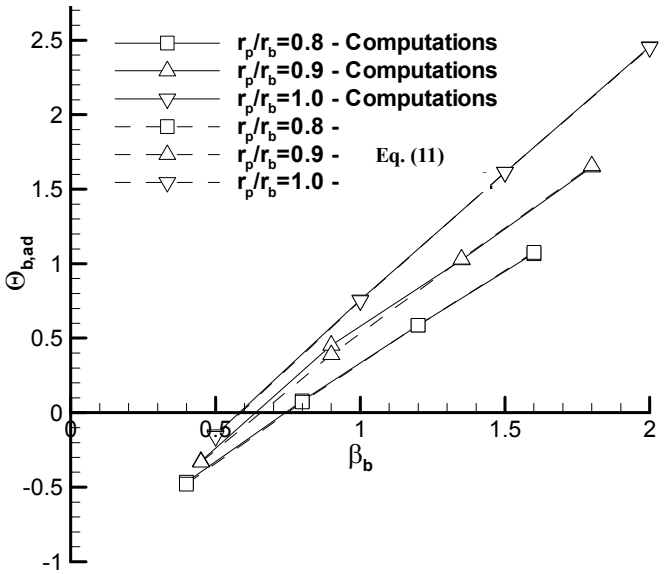

Fig. 10 Computed variation of adiabatic effectiveness $\Theta_{b,ad}$ with β_b

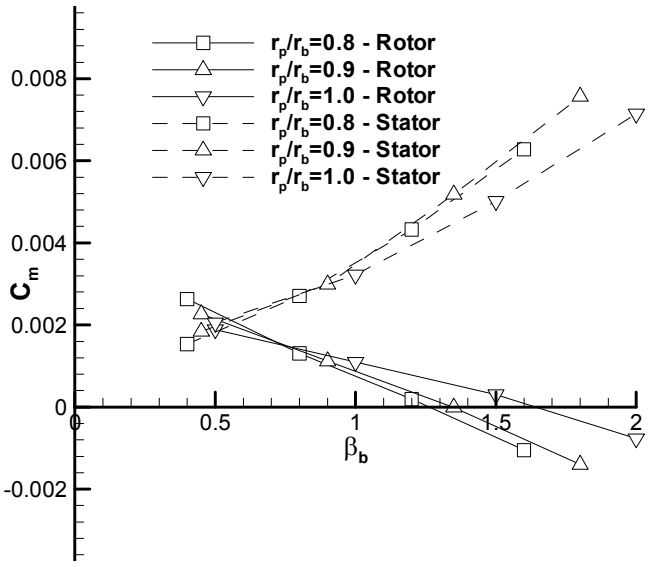

Fig. 11 Computed values of moment coefficient C_M on rotor and stator, $\lambda_T = 0.24$.

$$\Theta_{b,ad} = \frac{c_p(T_{o,p} - T_{t,b})}{1/2\Omega^2 r_b^2} \tag{9}$$

A theoretical value for $\Theta_{b,ad}$ was derived by Karabay et al [15] for a cover-plate system using the First Law of Thermodynamics. The equivalent theoretical expression derived by Farzeneh-Gord et al [5] for the direct-transfer system considered here is:

$$\Theta_{b,ad} = 2\beta_p \left(\frac{r_p}{r_b}\right)^2 - 1 - \frac{M_s}{1/2\dot{m}\Omega r_b^2} \tag{10}$$

When expressed in terms of β_b, the pre-swirl ratio based on the receiver-hole radius, this relationship becomes

$$\Theta_{b,ad} = 2\beta_b \frac{r_p}{r_b} - 1 - \frac{M_s}{1/2\dot{m}\Omega r_b^2} \tag{11}$$

Fig. 10 shows the computed effectiveness plotted against the relationship in eq. (11). Note that a computed moment on the stator is necessary to evaluate the relationship and hence only discrete values are available. The agreement between the two is excellent. As shown in the Appendix, in practice the increase of $\Theta_{b,ad}$ with increasing r_p will be less than that shown in Fig. 10.

For turbine blade cooling the effectiveness should be as high as possible as this ensures that the fluid reaching the blades has the lowest possible total temperature. In general, configurations with low pre-swirl ratios require work to be performed on the flow by the rotor to bring its tangential velocity to that of the receiver holes, and this work input raises the total temperature of the flow. Conversely, configurations with high pre-swirl ratios perform work on the rotor, thus reducing the total temperature.

As shown in eq. (11), the relationship between the pre-swirl ratio and the adiabatic effectiveness is approximately linear, with the gradient dependent on r_p/r_b. As the radius of the inlet increases there is consequently a resulting increase in effectiveness.

A secondary effect adding to the improvement in effectiveness for high radius inlets is the reduction in moment on the stator. This is shown in Fig. 11; as the pre-swirl ratio is increased, the moment on the stator increases and that on the rotor decreases. The change in moment coefficient is slightly less for $r_p/r_b = 1$ than for the other two locations.

CONCLUSIONS

The effect of nozzle location on the fluid dynamics of a pre-swirl system has been studied computationally. The model, which has been validated previously using an experimental rig at the University of Bath, produces a flow structure representative of that found in gas turbine engines.

Computations were performed at $Re_\phi = 10^6$, $0.12 < \lambda_T < 0.36$ and $0.5 < \beta_b < 2.0$.

The main conclusions from the study are:

1. $C_{d,b}$, the discharge coefficient for the receiver holes, is maximized when the core flow is in synchronous rotation with the holes ($\beta_\infty = 1$).
2. A simple model based on the effective receiver-hole area can be used to estimate the reduction in $C_{d,b}$ when $\beta_\infty \neq 1$.
3. The maximum $C_{d,b}$ is achieved at a value of β_b that decreases as r_p/r_b increases, with a corresponding slight increase in the pressure drop in the system.
4. The adiabatic effectiveness increases as r_p/r_b increases, and computed values are in excellent agreement with the theoretical analysis.

As shown in the Appendix, the variation of static pressure in the core will reduce, but will not negate, the advantages of locating the pre-swirl nozzles at as high a radius as practicable. It is also shown in the Appendix that the increase in effectiveness as r_p increases is caused solely by losses in the nozzles and in the core.

ACKNOWLEDGMENTS

The Engineering and Physical Sciences Research Council (EPSRC) sponsored Paul Lewis' research at the University of Bath through Doctoral Training Account EP/P500036/1. The authors thank the reviewers for comments that have given rise to improvements to the focus and completeness of the paper.

REFERENCES

[1] Meierhofer, B., and Franklin, C. J., 1981, "An investigation of a preswirled cooling airflow to a turbine disc by measuring the air temperature in the rotating channels," ASME Paper 81-GT-132.

[2] Wilson, M., Pilbrow, R., and Owen, J. M., 1997, "Flow and heat transfer in a pre-swirl rotor-stator system," ASME J. Turbomach., **119**, pp. 364–373.

[3] Geis, T., Dittmann, M., and Dullenkopf, K., 2004, "Cooling air temperature reduction in a direct transfer preswirl system," J. Engineering for Gas Turbines and Power, **126**, pp 809-815.

[4] Chew, J. W., Ciampoli, F., Hills, N. J., and Scanlon, T., 2005, "Pre-swirled cooling air delivery system performance," ASME Paper GT2005-68323.

[5] Farzaneh-Gord, M., Wilson, M., and Owen, J. M., 2005, "Numerical and theoretical study of flow and heat transfer in a pre-swirl rotor-stator system," ASME Paper GT2005-68135.

[6] Dittmann, M., Geis, T., Schramm, V., Kim, S., and Wittig, S., 2002, "Discharge coefficients of a preswirl system in secondary air systems," ASME J. Turbomach., **124**, pp. 119–124.

[7] Yan, Y., Farzaneh-Gord, M., Lock, G., Wilson, M., and Owen, J. M., 2003, "Fluid dynamics of a pre-swirl rotor-stator system," ASME J. Turbomach., **125**, pp. 641–647.

[8] Lewis, P., Wilson, M., Lock, G. D., and Owen, J., 2007. "Physical interpretation of flow and heat transfer in pre-swirl systems", J. Engineering for Gas Turbines and Power, **129**, pp 769-777

[9] Jarzombek, K, Benra, F.-K., H. Dohmen, J. and Schneider, O., 2007, "CFD analysis of flow in high-radius pre-swirl systems", ASME paper GT2007-27404

[10] Barth, T. J., and Jesperson, D. C., 1989, "The design and application of upwind schemes on unstructured meshes," Proc. 27th AIAA Aerospace Sciences Meeting, Reno, NV, January 9–12.

[11] Menter, F. R., 1994, "Two-equation eddy viscosity turbulence models for engineering applications," AIAA J., **32**, pp. 269–289.

[12] Wilcox, D. C., 1998, "Turbulence modelling for CFD", 2nd ed., DCW Industries, La Canada, CA.

[13] Mirzaee, I., Gan, X., Wilson, M. and Owen, J. M., 1998, "Heat transfer in a rotating cavity with a peripheral inflow and outflow of cooling air", ASME J. Turbomach, **120**, pp 818-823

[14] Owen, J. M. and Rogers, R. H., 1989, "Flow and heat transfer in rotating-disc systems (vol. 1 Rotor-stator systems)", Research Studies Press, Taunton, UK

[15] Karabay, H., Wilson, M., and Owen, J. M., 2001, "Predictions of effect of swirl on flow and heat transfer in a rotating cavity," Int. J. Heat Fluid Flow, **22**, pp. 143–155.

APPENDIX: EFFECT OF CORE SWIRL ON PRE-SWIRL RATIO

If V_T is the total velocity leaving the nozzles, then for *incompressible flow*

$$V_T = C_{d,p}\left[\frac{2(p_0 - p_p)}{\rho}\right]^{1/2} \qquad \text{(A1)}$$

where p_0 is the total pressure upstream of the nozzles, p_p is the static pressure in the core at the radius of the nozzles, $C_{d,p}$ is the discharge coefficient for the nozzles, and

$$V_T = \frac{V_{\phi,p}}{\cos\theta} = \frac{\beta_b \Omega r_b}{\cos\theta} \qquad \text{(A2)}$$

θ being the nozzle angle to the tangential direction. Hence

$$\beta_b = \frac{C_{d,p}\cos\theta}{\Omega r_b}\left\{\frac{2(p_0 - p_p)}{\rho}\right\}^{1/2} \qquad \text{(A3)}$$

If $\beta_{b,1}$ is the value of β_b when $r_p/r_b = 1$, it follows that

$$\beta_{b,1} = \frac{C_{d,p}\cos\theta}{\Omega r_b}\left\{\frac{2(p_0 - p_b)}{\rho}\right\}^{1/2} \tag{A4}$$

and hence

$$\frac{\beta_b}{\beta_{b,1}} = \left\{1 - \frac{{C_{d,p}}^2 \cos^2\theta (p_b - p_p)}{1/2\,\rho\,{\beta_b}^2 \Omega^2 {r_b}^2}\right\}^{-1/2} \tag{A5}$$

Consider a combined vortex in the core, as shown in Fig. 5, where

$$\frac{V_\phi}{\Omega r} = A + B\left(\frac{r}{b}\right)^{-2} \tag{A6}$$

It follows that

$$\frac{dp}{dr} = \rho\frac{{V_\phi}^2}{r} = \rho\Omega^2 r\left\{A^2 + 2AB\left(\frac{r}{b}\right)^{-2} + B^2\left(\frac{r}{b}\right)^{-4}\right\} \tag{A7}$$

Integrating from $r = r_p$ to $r = r_b$

$$p_b - p_p = \frac{1}{2}\rho\Omega^2 {r_b}^2 \times \left\{\begin{array}{l} A^2\left(1 - \frac{{r_p}^2}{{r_b}^2}\right) - 4AB\left(\frac{r_b}{b}\right)^{-2}\ln\left(\frac{r_p}{r_b}\right) \\ \quad + B^2\left(\frac{r_b}{b}\right)^{-4}\left[\left(\frac{r_p}{r_b}\right)^{-2} - 1\right] \end{array}\right\} \tag{A8}$$

and from eq (A5)

$$\frac{\beta_b}{\beta_{b,1}} = \left\{1 - \frac{{C_{d,p}}^2\cos^2\theta}{{\beta_b}^2} \times \left(A^2\left(1 - \frac{{r_p}^2}{{r_b}^2}\right) - 4AB\left(\frac{r_b}{b}\right)^{-2}\ln\left(\frac{r_p}{r_b}\right) + B^2\left(\frac{r_b}{b}\right)^{-4}\left[\left(\frac{r_p}{r_b}\right)^{-2} - 1\right]\right)\right\}^{-1/2} \tag{A9}$$

The results corresponding to Fig. 5 are shown in Table A1 for an assumed value of $C_{d,p} = 0.9$ and $\theta = 20^o$, which corresponds to the nozzle angle in the experimental rig.

Consider the *ideal case* where $C_{d,p} = 1$, $\theta = 0$ and free-vortex flow occurs in the core, such that $A = 0$ and

$$\frac{V_\phi}{\Omega r} = B\left(\frac{r}{b}\right)^{-2} \tag{A10}$$

It follows that

$$\frac{V_{\phi,p}}{\Omega r_p} = B\left(\frac{r_p}{b}\right)^{-2} \tag{A11}$$

and

$$\beta_b = \frac{V_{\phi,p}}{\Omega r_b} = B\left(\frac{r_p\, r_b}{b^2}\right)^{-1} \tag{A12}$$

Hence

$$B = \beta_b \frac{r_p r_b}{b^2} \tag{A13}$$

and eq (A9) reduces to

$$\frac{\beta_b}{\beta_{b,1}} = \frac{r_b}{r_p} \tag{A14}$$

Reference to eq (11) shows that for this ideal case (where $\beta_b r_p/r_b$ is constant) the nozzle location has no effect on the adiabatic effectiveness! However, Table A1 shows that for the real case, although the core swirl reduces the advantage, the effectiveness increases as r_p increases. *It can therefore be concluded that the increase in effectiveness as r_p increases is caused solely by losses in the nozzles and in the core.*

r_p / r_b	0.8				0.9			
β_b	0.40	0.80	1.20	1.60	0.45	0.90	1.35	1.80
A	0.17	0.32	0.42	0.43	0.31	0.35	0.46	0.49
B	0.13	0.21	0.32	0.48	0.11	0.28	0.43	0.62
$\beta_b / \beta_{b,1}$	1.12	1.09	1.08	1.07	1.08	1.05	1.04	1.04

Table A1 Effect of core swirl on $\beta_b / \beta_{b,1}$ according to eq (A9) with $\theta = 20^0$ and $C_{d,p} = 0.9$.